

Optimal Control of Redundant Muscles in Step-Tracking Wrist Movements

Masahiko Haruno and Daniel M. Wolpert

JN 94:4244-4255, 2005. First published Aug 3, 2005; doi:10.1152/jn.00404.2005

You might find this additional information useful...

This article cites 26 articles, 11 of which you can access free at:

<http://jn.physiology.org/cgi/content/full/94/6/4244#BIBL>

Updated information and services including high-resolution figures, can be found at:

<http://jn.physiology.org/cgi/content/full/94/6/4244>

Additional material and information about *Journal of Neurophysiology* can be found at:

<http://www.the-aps.org/publications/jn>

This information is current as of January 21, 2006 .

Optimal Control of Redundant Muscles in Step-Tracking Wrist Movements

Masahiko Haruno^{1,2} and Daniel M. Wolpert¹

¹Sobell Department of Motor Neuroscience and Movement Disorders, Institute of Neurology, University College London, Queen Square, London, United Kingdom; and ²Computational Neuroscience Laboratories, Advanced Telecommunications Research Institute, Kyoto, Japan

Submitted 20 April 2005; accepted in final form 2 August 2005

Haruno, Masahiko and Daniel M. Wolpert. Optimal control of redundant muscles in step-tracking wrist movements. *J Neurophysiol* 94: 4244–4255, 2005. First published August 3, 2005; doi:10.1152/jn.00404.2005. An important question in motor neuroscience is how the nervous system controls the spatiotemporal activation patterns of redundant muscles in generating accurate movements. The redundant muscles may not only underlie the flexibility of our movements but also pose the challenging problem of how to select a specific sequence of muscle activation from the huge number of possible activations. Here, we propose that noise in the motor command that has an influence on task achievement should be considered in determining the optimal motor commands over redundant muscles. We propose an optimal control model for step-tracking wrist movements with redundant muscles that minimizes the end-point variance under signal-dependent noise. Step-tracking wrist movements of human and nonhuman primates provide a detailed data set to investigate the control mechanisms in movements with redundant muscles. The experimental EMG data can be summarized by two eminent features: 1) amplitude-graded EMG pattern, where the timing of the activity of the agonist and antagonist bursts show slight variations with changes in movement directions, and only the amplitude of activity is modulated; and 2) cosine tuning for movement directions exhibited by the agonist and antagonist bursts, and the discrepancy found between a muscle's agonist preferred direction and its pulling direction. In addition, it is also an important observation that subjects often overshoot the target. We demonstrate that the proposed model captures not only the spatiotemporal activation patterns of wrist muscles but also trajectory overshooting. This suggests that when recruiting redundant muscles, the nervous system may optimize the motor commands across the muscles to reduce the negative effects of motor noise.

INTRODUCTION

A remarkable feature in our daily lives is our ability to effortlessly achieve precise movements, such as reaching and grasping, by controlling a set of redundant muscles. It is a fundamental question in motor neuroscience how the nervous system controls the spatiotemporal activation pattern across redundant muscles. Although this redundancy of muscles is the source of flexibility and adaptability of our motor control system, it also causes the so-called *ill-posedness problem*, where there are infinite possible solutions that could achieve the goal of a movement (Bernstein 1967). However, it is often observed that spatiotemporal patterns of both muscle recruitment and kinematics of movements are highly stereotyped within and between individuals. Good examples of this stereotypy are the two peaks observed in agonist and antagonist

EMG waveforms and bell-shaped velocity profile (Berardelli et al. 1996; Hollerbach and Atkeson 1987).

In the field of reaching movements, many optimal control models have been proposed to solve the problem of trajectory redundancy. Flash and Hogan (1985) and Uno et al. (1989) both noticed the smoothness of trajectory plays a crucial role in trajectory planning, suggesting minimum jerk criterion and minimum torque change criterion, respectively. In contrast, the minimization of end-point variance under signal-dependent noise (SDN) not only explained the key features of reaching, but also provided a unified theoretical framework for both arm reaching and saccadic eye movements (Harris and Wolpert 1998). SDN proposes that the motor command is corrupted by noise at the muscle level and the amount of noise scales with the magnitude of the original motor command. Although these models of trajectory planning have so far focused on joint torques, the SDN model is a promising candidate to explain the spatiotemporal pattern of redundant muscle recruitment because SDN itself originates from muscle activity (Hamilton et al. 2004; Jones et al. 2002). In this paper, we propose an optimal control model for the step-tracking wrist movement that minimizes the end-point variance under SDN and demonstrate that the proposed model captures the key spatiotemporal characteristics of both redundant muscles' activity and trajectory. This is consistent with the view that the nervous system uses an optimal control principle, at least in an abstract level, to recruit the redundant muscles to achieve accurate movements.

The step-tracking wrist movement that has been intensively studied by Hoffman and Strick (1986, 1990, 1993, 1999) provides an important data set for investigations of the spatiotemporal activation pattern of redundant muscles. The task requires subjects to make point-to-point wrist movements. Radial/ulnar deviation and extension/flexion of the wrist are mapped onto two orthogonal axes and determine the movement of a cursor on a screen. Subjects start in a central neutral position and make movement to one of 12 targets arranged on a circle (Fig. 1A). EMG activity is recorded from five wrist muscles: extensor carpi radialis longus (ECRL), extensor carpi radialis brevis (ECRB), extensor carpi ulnaris (ECU), flexor carpi radialis (FCR), and flexor carpi ulnaris (FCU). In monkeys the pulling direction of these five muscles is determined as the direction of wrist movement elicited by electrical stimulation of that muscle in isolation (Fig. 1B).

The data demonstrate three characteristic features in the spatiotemporal patterns of muscle activity: 1) amplitude-graded EMG patterns, where the amplitude of EMG activity

Address for reprint requests and other correspondence: M. Haruno, Department of Cognitive Neuroscience, ATR Computational Neuroscience Labs, 2-2-2 Hikaridai Seikacho, Sorakugun, Kyoto 619-0288, Japan (E-mail: mharuno@atl.2p).

The costs of publication of this article were defrayed in part by the payment of page charges. The article must therefore be hereby marked "advertisement" in accordance with 18 U.S.C. Section 1734 solely to indicate this fact.

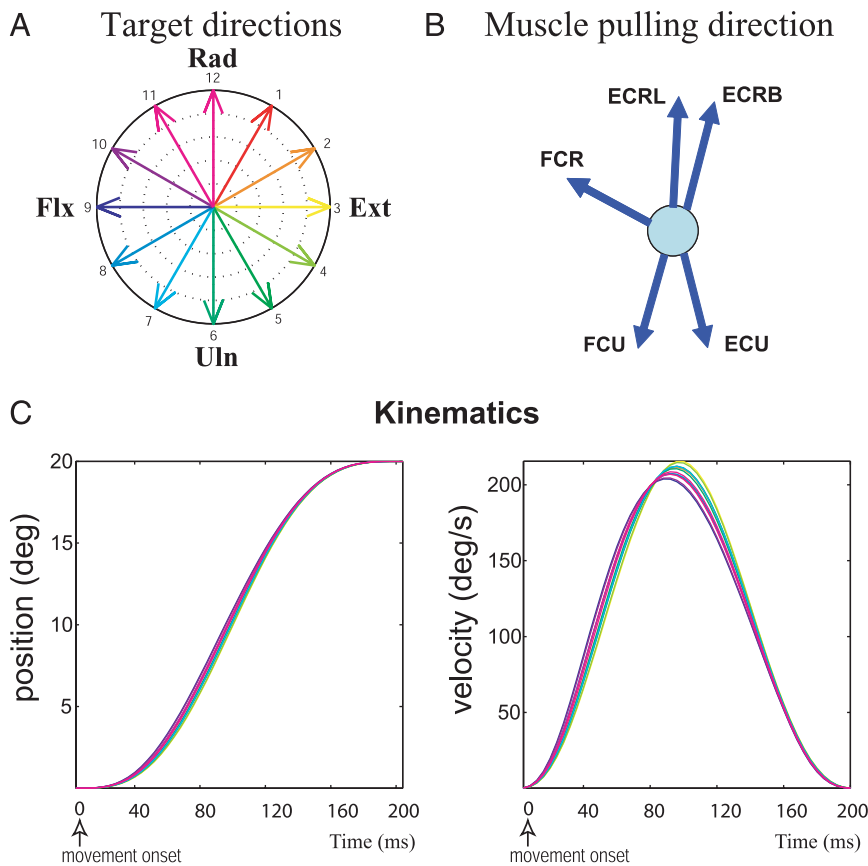


FIG. 1. Step-tracking wrist movement. *A*: forelimb was held in the neutral position, midway between full pronation and full supination. To initiate a trial, the subject placed the cursor at the center of the screen corresponding to the wrist's being in a neutral position. After a variable hold period, the subject was required to move the cursor to one of 12 different targets as rapidly and accurately as possible. Zero degrees is in the up direction and degrees increase in the clockwise direction. *B*: muscle pulling directions for extensor carpi radialis longus (ECRL), extensor carpi radialis brevis (ECRB), extensor carpi ulnaris (ECU), flexor carpi ulnaris (FCU), and flexor carpi radialis (FCR) muscles were 1.6, 18.4, 159.5, 198.3, and 304.5°, respectively. Data were the average of 2 monkeys (PL Strick, DS Hoffman, and S. Kakei, personal communication). *C*: simulated trajectories and velocity profiles obtained when the target was varied from 1 to 12. Colors represent the target directions depicted in *A*.

varies over the movement direction but, in contrast, the timing of the activity shows little variation with movement direction. 2) Cosine tuning of both agonist and antagonist bursts over the movement directions. 3) Deviation of the preferred directions (peak in the cosine tuning) of each muscle from their pulling directions. It is also noteworthy that both human and monkey subjects often overshoot the targets.

Previous computational studies have tried to determine the average EMG activity over a movement controlled by set of redundant muscles. Buchanan and Shreeve (1996) compared a number of criteria of effort minimization such as squared force, squared normalized force, and squared and cubed stress and reported that only slight differences were found in the predicted EMG pattern. Similarly, Fagg et al. (2002) and Shah et al. (2004) proposed a model of muscle recruitment in the step-tracking wrist movement that minimized the sum of squared muscle activation. The model succeeded in demonstrating cosine-like recruitment pattern of agonist EMG and also the discrepancy between the muscle's pulling and preferred direction. Todorov (2002) also pointed out the relevance of signal-dependent noise to cosine tuning in the isometric case. However, these models focused only on the average activity over agonist bursts, and can explain neither the spatiotemporal characteristics of redundant muscle recruitment nor the characteristics of trajectories.

Here we examine a model in which the motor commands in each muscle are corrupted by signal-dependent noise and the optimal strategy is to use the muscle activations that minimize the variance of terminal error. This model allows a prediction of the spatiotemporal EMG of the muscles and we show that it captures all of the main features seen in the human and monkey

data, which include amplitude-graded EMG pattern in agonist and antagonist EMG bursts, cosine tuning in agonist and antagonist EMG bursts, asymmetry between preferred directions and pulling directions, and overshooting in the trajectory.

METHODS

Optimal control model

We set out to determine the optimal sequence of motor commands to apply to the five muscles to achieve the task as accurately as possible. More concretely, we propose that the movements start stationary and that a feedforward motor command is selected for each muscle so that the movement on average ends stationary on the target and, in addition, the motor commands are chosen to minimize the final variance of the movement, thereby generating the most accurate movement possible. In the following, we first provide the model description. Then, we describe the relationship between the motor command sequence and the average kinematics and its variance under SDN. Finally, we derive the optimization procedure for the final variance to find the optimal motor commands.

First, the wrist position is denoted as $\{x(t), y(t)\}$, where $x(t)$ represents flexion–extension and $y(t)$ radial–ulnar deviation at time t . The position of the wrist is determined by the activation of five muscles, ECRL, ECRB, ECU, FCU, and FCR, each of which is controlled by its own motor command $u_i(t)$ ($i = 1 \dots 5$, respectively). Each muscle acts with a fixed pulling direction α_i , representing the angle between the i th muscle and the y -axis. The pulling angles α_i for each muscle were set to [1.6, 18.4, 159.5, 198.3, 304.5] degrees (positive angles are taken as clockwise; Fig. 1A) following the averaged data of two monkeys (PL Strick, DS Hoffman, and S. Kakei, personal communication). For a parsimonious and tractable model, we use linear systems for muscles and dynamics. Each muscle is modeled as an identical second-order linear system following Van der Helm

and Rozendaal (2000) that converts motor commands into output force with time constants of 30 and 40 ms, representing excitation and activation, respectively. The wrist dynamics is also modeled as a linear system, whose parameters were selected within a biologically plausible range to reasonably reproduce experimental data. The measured moment of inertia of the wrist and manipulandum during stabilization of a wrist targeted movement ranges from 0.00322 to 0.00541 kgm² with an average of 0.00469 kgm² (Grey 1997). A similar value was also reported in Milner and Cloutier (1998). Although the viscosity and stiffness of the wrist still remain to be fully measured, the natural viscosity of the relaxed wrist was estimated to be 0.02–0.03 Nms/rad (Gielen and Houk 1984), consistent with the average viscosity of 0.03 Nms/rad estimated in the above stabilization study (Grey 1997). The stiffness for the relaxed wrist was estimated to be between 0.3 and 3 Nm/rad (de Serres and Milner 1991; Gielen and Houk 1984). In contrast, the stiffness of the wrist during stabilization of a target movement was reported to be 6.3 on average (Grey 1997), consistent with another study from the same group (Milner and Cloutier 1998). Considering these experimental measurements, in our main simulations, we used moment of inertia $m = 0.005$ kgm², viscosity $b = 0.03$ Nms/rad, and stiffness $k = 0.1$ Nm/rad. In the overshooting simulation, the viscosity and stiffness were set to $b = 0.15$ Nms/rad and $k = 4.0$ Nm/rad, respectively. These two sets of the parameters would be plausible because the stiffness and the viscosity scale with muscle activation by comparable amounts. In addition to these values used in our main simulations, we systematically investigated how the simulated EMG and trajectory changes when the stiffness and viscosity are varied.

Second, we describe the relationship between the motor command sequence and the average kinematics and positional variance under SDN. We model the effect of each muscle acting alone on the wrist by using an impulse response $p(t)$, which represents the combined dynamic behavior of the muscle and wrist along the muscles, pulling direction. The impulse response is the positional trace of the wrist when an impulse is given as the motor command. To represent signal-dependent noise on the motor commands, we assume that each motor command is corrupted by Gaussian noise with zero mean (unbiased) and the SD proportional to the absolute value of motor command. That is, the SD is represented as $\sigma_{u_i}(t) = k |u_i(t)|$, where k is the coefficient of variation and is assumed to be the same for all five muscles. Because the system is linear, the effect of all the muscles can be modeled by simply summing their individual effects modified by their pulling direction in the x and y -directions. Because the noise on the motor command is unbiased and therefore has no effect on average kinematics, we can calculate the average kinematics of the movement at time t as the following sums of convolutions

$$E[x^{(n)}(t)] = \sum_{i=1}^5 \sin \alpha_i \int_0^t u_i(\tau) p^{(n)}(t - \tau) d\tau \quad (1)$$

$$E[y^{(n)}(t)] = \sum_{i=1}^5 \cos \alpha_i \int_0^t u_i(\tau) p^{(n)}(t - \tau) d\tau$$

where the superscript n refers to the n th derivative of the position variables (i.e., velocity, acceleration, and so forth). Substituting the signal-dependent SD above, the variance of the wrist position at time t amounts to the following

$$\sigma_x^2(t) = \text{Var}[x(t)] = \sum_{i=1}^5 \sin^2 \alpha_i \int_0^t \text{Var}[u_i(\tau)] p^2(t - \tau) d\tau$$

$$= \sum_{i=1}^5 \sin^2 \alpha_i \int_0^t k^2 u_i^2(\tau) p^2(t - \tau) d\tau$$

$$\sigma_y^2(t) = \text{Var}[y(t)] = \sum_{i=1}^5 \cos^2 \alpha_i \int_0^t \text{Var}[u_i(\tau)] p^2(t - \tau) d\tau$$

$$= \sum_{i=1}^5 \cos^2 \alpha_i \int_0^t k^2 u_i^2(\tau) p^2(t - \tau) d\tau$$

Finally, our task is now to find an optimal motor command that not only moves the wrist to the target on average but also minimizes the end-point variances. Corresponding to these two requirements, we apply both a constraint and a cost on the movement. The constraint is on the kinematic boundary conditions at the start ($t = 0$) and end ($t = M$) of the movement. Specifically, these constraints require that the wrist starts stationary at the central start position and ends on average stationary on the target. Therefore, $E[x^{(0)}(M)] = x^*$, $E[y^{(0)}(M)] = y^*$ and $x^{(n)}(M) = y^{(n)}(M) = 0$ for $n = 1 \dots 3$, where x^* and y^* correspond to targets 1 to 12 that are each 20° from the starting location. The cost is the sum of end-point variance of the movements over an F ms postmovement period

$$\text{Cost} = \int_M^{M+F} \sigma_x^2(t) + \sigma_y^2(t) dt = k^2 \sum_{i=1}^4 \int_M^{M+F} \int_0^t u_i^2(\tau) p^2(t - \tau) d\tau dt \quad (2)$$

It is obvious from Eq. 2 that the coefficient k (provided it is >0) will not affect the selection of optimal control because it is simply a scaling factor on the cost. Therefore, we set k to 1 for simplicity. In addition, closely related to the minimum variance model under SDN, the minimum energy consumption criterion minimizes the total energy during movement, which is the integral of squared motor commands over the movement. This constraint can be easily represented by replacing $p(t - \tau)$ with 1 in Eq. 2. We will later discuss the similarity and difference arising from these two constraints.

Because Eq. 2 is a quadratic form in $u_i(t)$, the minimization can be solved with quadratic programming (cf. MINQ, Neumaier 1998) with an additional constraint that $u_i(t)$ must be positive, ensuring that the muscles can only pull. We set the movement time M to 200 ms and the postmovement time F to 500 ms. The movement time was chosen to match the average movement duration seen in human and monkey data (Hoffman and Strick 1999) and the selection of F had little effect on results when it was >200 ms. A sampling interval of 4 ms was used throughout simulations. The basic algorithm for the optimal control model is presented as MATLAB code in the APPENDIX.

Calculation of directional tuning

The optimization process generates the five optimal motor commands for each muscle as a function of time. Simulated EMGs were generated by applying a fifth-order 20-Hz low-pass Butterworth filter to each motor command $u_i(t)$. The agonist and antagonist directional tuning was computed from the temporal waveform of EMG following a data analysis similar to that in Hoffman and Strick (1999). To perform this analysis, a time window is defined for the agonist and antagonist burst of each muscle and for each direction. The integrated EMG activity in the window is taken as a measure of muscle activity. To set the interval, we first determined the movement direction with the largest agonist burst (best agonist direction) and largest antagonist burst (best antagonist direction) for each muscle. This allowed us to define agonist and antagonist burst thresholds for each muscle, taken as 25% of the peak amplitude of the muscle's largest bursts (Hoffman and Strick 1999). These thresholds were then used to specify the start and end of the EMG burst for other directions. Thus the time window used for integration was allowed to vary for different directions of movement. To prevent agonist and antagonist burst intervals from overlapping, their respective intervals were always limited to -20 to $+60$ ms and $+70$ to $+150$ ms in reference to movement onset, respectively. The integrated simulated EMG activity (E) was fit by a

cosine-tuning function of direction. That is, in accordance with Hoffman and Strick (1999) and Georgopoulos et al. (1982), the regression equation was $E = a + b \sin(\phi) + c \cos(\phi)$, where ϕ represented movement direction in radians and a , b , and c were regression coefficients. The preferred direction (PD) is defined as the peak of the cosine for each muscle's agonist or antagonist activity.

RESULTS

Kinematics and spatiotemporal patterns of EMG

Figure 1C shows the trajectories and velocity profiles predicted by the model for optimal movements to the 12 different target directions. In all directions, the movement trajectory was found to be smooth and the velocity profile was symmetric and bell-shaped. The figure confirms that the optimal control on average achieves the task perfectly in all target directions.

Figure 2 shows the spatiotemporal profiles of the five muscles' EMG (filtered version of the optimal motor commands sequences) for the optimal movements. The EMG colors correspond to the colors for the target direction in Fig. 1A. It can be seen that each muscle shows agonist bursts for some directions (e.g., target 1 light red for ECRL) and antagonist bursts for other directions (e.g., target 7 blue for ECRL). When the target was varied from 1 to 12, the predicted agonist and antagonist EMG activity of all the muscles changed only in amplitude but not in their timing. Therefore the model exhibits the amplitude-graded EMG pattern in both agonist and antagonist burst intervals. In the following discussion, we will mainly focus on ECRL, ECRB, ECU, and FCR because data for FCU are inactive in monkeys and were unstable in the

human experiments and therefore do not allow us to compare data from simulation and experiment.

Figure 3A shows a subset of the data for ECRL and ECU from Fig. 2 together with the equivalent empirical EMG data of human subjects in Fig. 3B. For the directions in which ECRL and ECU act as agonists, we see two agonist bursts predicted that are modulated in amplitude, as seen in the empirical data. Examination of the antagonist activity showed a similar amplitude-graded pattern. The order of the amplitude modulation over the direction shown in Fig. 2B is seen in both muscles and directions. The only notable difference between the simulation and experimental data was the antagonist activity for ECU for direction 1 in which the activity was largest in the experimental data but second in the simulation. This difference might arise from the fact that we used pulling-direction data taken from monkeys to simulate experimental data from human subjects.

Directional tuning in agonist and antagonist EMG

To investigate how the simulated amplitude-graded EMG is modulated in accordance with the change in target direction, we calculated directional tuning for both agonist and antagonist activity and fit them with a cosine-tuning function of movement direction. Each black point in Fig. 4 illustrates the integrated EMG activity for one target direction during the first agonist (*top*) and antagonist (*bottom*) burst intervals (see also *methods*). The *top* and *bottom* lines show the fit of the cosine function demonstrating the modulation in amplitude of the agonist and antagonist EMG with direction, respectively. The average r^2 values for the fits to the agonist and antagonist activity were 0.86 and 0.87, respectively. The preferred directions (PD, i.e., the peak direction of cosine-fitting curve) of ECRL, ECRB, ECU, and FCR for agonist and antagonist activity were (13.4, 72.6, 109.0, and 278.1) and (194.2, 249.7, 291.2, and 97.0) degrees, respectively.

The same data are also plotted in polar coordinates in Fig. 5A, in which the short arrow represents each muscle's pulling directions, and thick and thin longer arrows show the agonist and antagonist PDs, respectively. Correspondingly, in the experimental data shown in Fig. 5B (human) and 5C (monkey), the black circles illustrate the change of agonist EMG with target direction, and long and short (in monkey data) arrows show the agonist PD and each muscle's pulling directions, respectively. The simulated data demonstrate several key characteristics of the experimental data. First, the agonist PD for each muscle is not coaligned with the muscle's pulling direction (short black arrows in Fig. 5A, and C; they are slightly different because average data of two monkeys was used in simulations). The difference in angular direction between the preferred direction in the simulations and the muscles' pulling direction was especially large in ECRB and ECU compared to that of ECRL and FCR. A similar discrepancy between the muscles is also seen in human (Fig. 5B) and monkey experimental data (Fig. 5C). The difference between the muscles' pulling and preferred direction likely originates from the anisotropic distribution of the muscles' pulling directions as also suggested in Fagg et al. (2002). ECRB and ECU need to be active for rightward movements because there is no muscle that pulls purely in this extension direction (in the direction of target 3). Second, the tuning curves in human data are broader than those in monkey data (Hoffman and Strick 1999). The

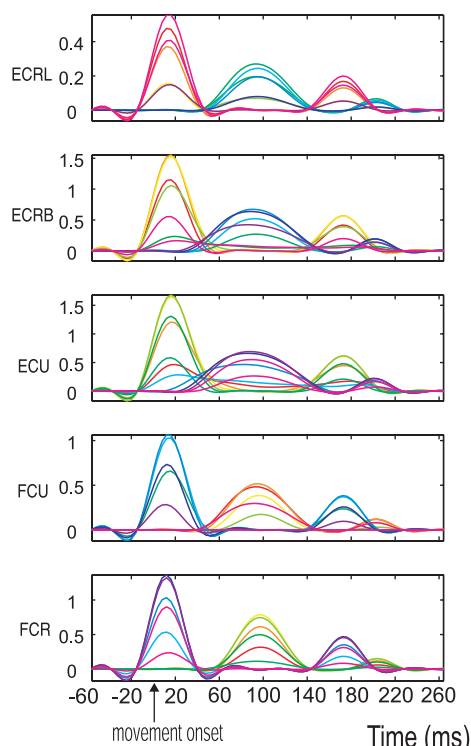


FIG. 2. Time course of predicted electromyogram (EMG). Predicted temporal waveforms of EMG for ECRL, ECRB, ECU, FCU, and FCR. Colors in the graph delineate the target directions, corresponding with Fig. 1A. Small negative values of EMG originated from the application of a Butterworth low-pass filter to the motor commands, which were all positive.

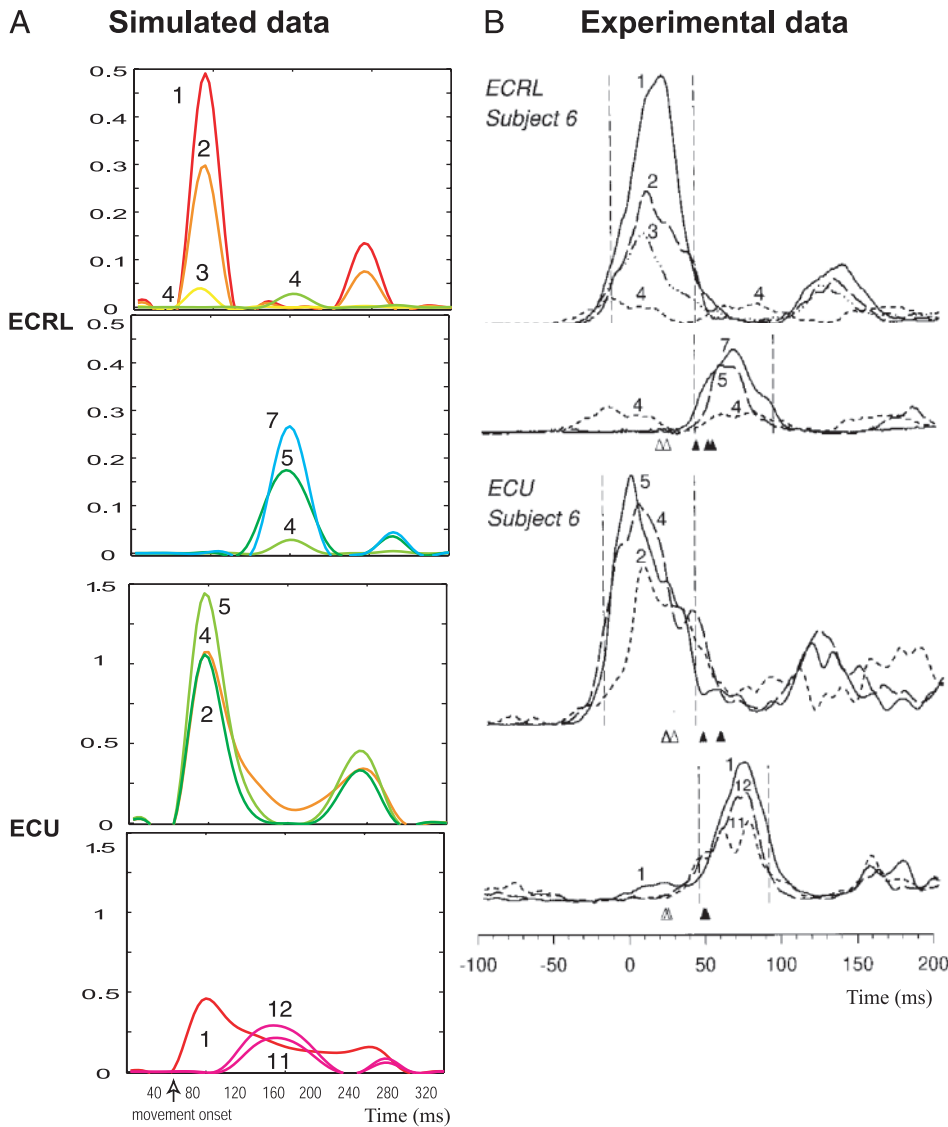


FIG. 3. Time course of predicted and experimental EMGs. A: predicted EMG for ECRL and ECU to illustrate the close correspondence with B. Data shown are a subset of Fig. 2. B: EMG data of ECRL and ECU experimentally recorded during step-tracking wrist movement (see Fig. 3 in Hoffman and Strick 1999). These data were taken from a human subject, but monkey subjects also exhibited a similar EMG pattern.

simulation exhibits a good agreement with human data, particularly for ECRL and ECRB. This may arise because these two muscles are needed to compensate for FCU in the vertical and horizontal direction, respectively. Third, even for directions in which a single muscle could act alone, coactivation of wrist

muscles is seen. In most target directions, at least two muscles were activated during the agonist burst interval. For instance, three wrist extensors ECRL, ECRB, and ECU, were coactivated when human subjects moved the wrist to targets 1 and 2. In contrast, a wrist extensor ECRL and a wrist flexor FCR were

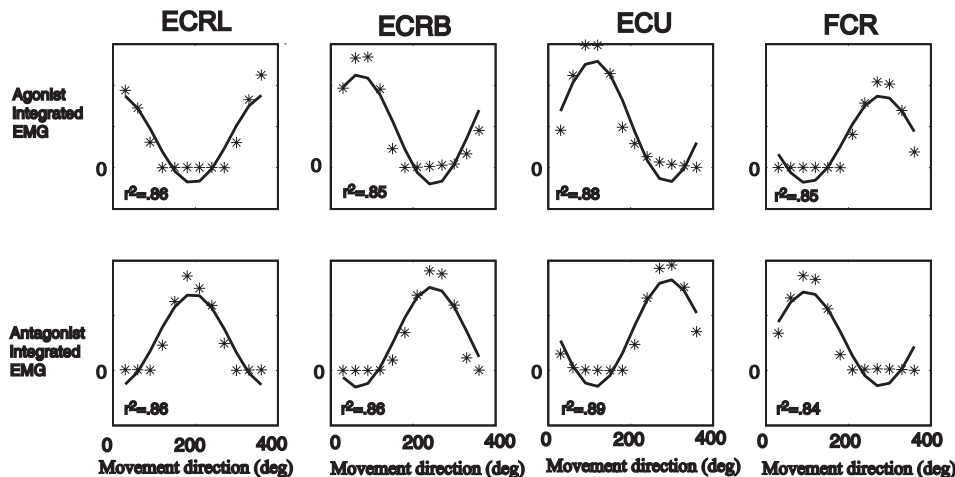


FIG. 4. Cosine fitting of integrated EMG during agonist or antagonist burst intervals. Each point shows an integrated EMG of one muscle for one of 12 target directions. Goodness of fit, measured by r^2 , is displayed in the figure.

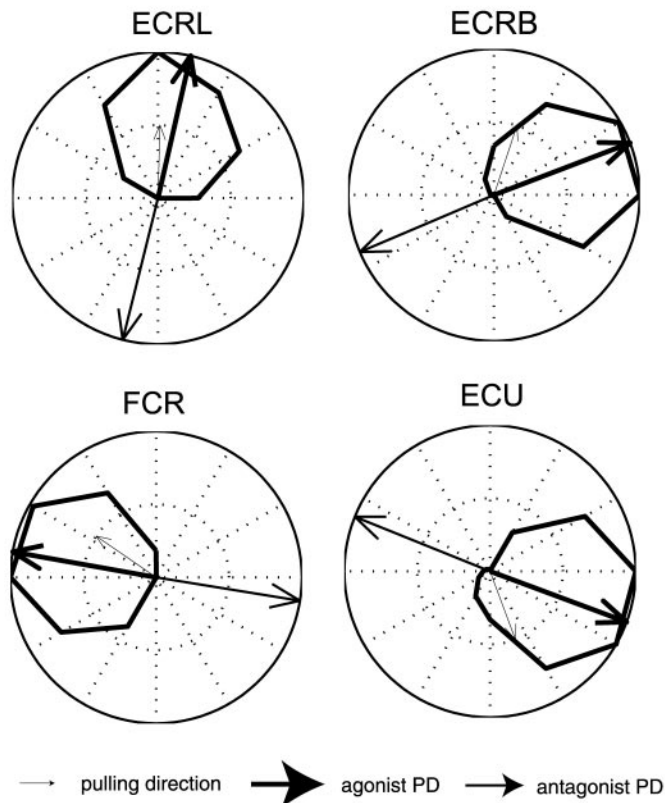
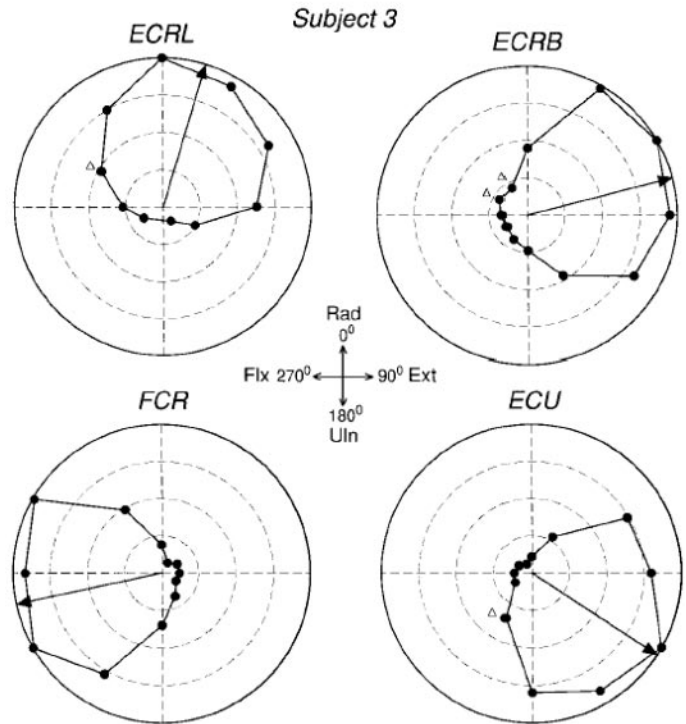
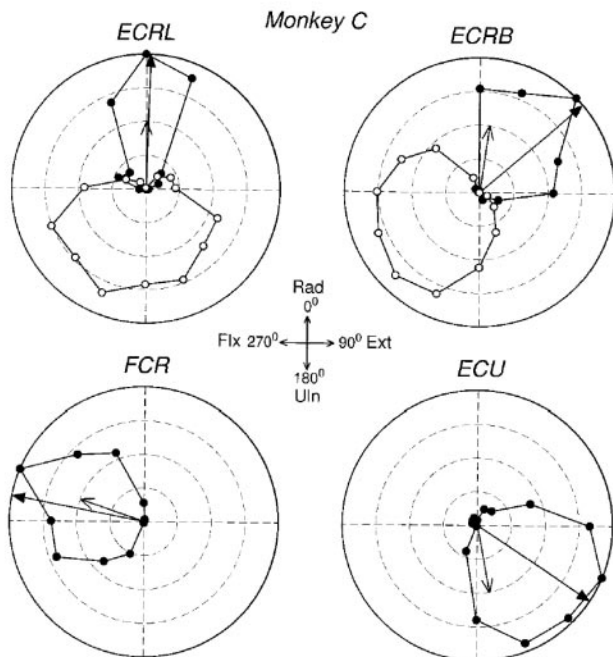
A Directional tuning (simulation)**B Directional tuning (human)****C Directional tuning (monkey)**

FIG. 5. Directional tuning of agonist and antagonist EMG. *A*: activation in predicted EMG. Thick curve depicts the integrated agonist EMG that was obtained from the simulation. Short arrow represents each muscle's pulling directions, and thick and thin long arrows show the agonist and antagonist preferred directions (PDs), respectively. *B* and *C*: activation patterns in experimentally measured EMG that were taken from a human (*B*) (Fig. 6 in Hoffman and Strick 1999) and a monkey (*C*) (Fig. 12 in Hoffman and Strick 1999). Black circles depict the integrated agonist EMG with varied target directions, and short and long arrows show each muscle's pulling direction and the agonist PD, respectively. In monkey data (*C*), open circles show the decrease of agonist EMG that we did not consider in simulation.

coactivated when the wrist was moved to target 11. Thus, the proposed optimal control model reproduces the experimental coactivation pattern during agonist burst interval that included not only the muscles that are normally considered as synergists (ECRL, ECRB, and ECU) but also those that are normally regarded as antagonists (ECRL and FCR).

Minimum energy consumption constraint

It is interesting to compare the minimum-variance model we have so far focused on with the minimum energy consumption model. We conducted the simulations with the same constraints but for a cost that minimizes the energy of the movement (see METHODS). The spatiotemporal patterns of simulated EMG turned out to be almost the same as those with the minimum variance (c.f. Fig. 2), demonstrating the amplitude-graded pattern, as well as two agonist and antagonist peaks. Furthermore, the tuning patterns of agonist and antagonist EMG generated by these two models exhibited no significant difference. More specifically, the preferred directions of ECRL, ECRB, ECU, and FCR for agonist and antagonist activity were (13.4, 72.9, 108.8, and 278.0) and (194.0, 249.1, 292.0, and 97.0) degrees, respectively.

Overshooting as an optimal control strategy

In fast wrist movements, it is often observed that subject's trajectory overshoots the target (Berardelli 1996; Hoffman and Strick 1999; Milner 2002; Mustard 1987). An interesting computational question here is whether such overshooting could be an optimal control strategy to minimize end-point error, or a sub-optimal strategy induced by the rapidity of the movement. To address this question, we investigated whether the current optimal model can predict target overshooting. Figure 6A shows the trajectories and velocity profiles predicted by the minimum-variance model under SDN for optimal movements when the stiffness and viscosity of the wrist are increased in an appropriate level for overshooting (see METHODS). The stiffness and viscosity of the wrist are likely to increase with cocontraction. In this case, the optimal strategy in the current model was to overshoot the target before returning to it. The comparison of Figs. 1C and 6A shows that the velocity in the latter case reaches its maximum earlier in the movement, then sharply decreases to show a reversal of velocity that peaks and slowly shifts back to 0. Figure 6B displays the corresponding EMG activity obtained in the simulation. Importantly, amplitude-graded agonist and antagonist EMG as well as two peaks of agonist EMG are evident. The pattern of trajectory and EMG indicates that the model first uses the agonist force to accelerate the wrist; then, it decelerates the wrist by the antagonist force; and finally used the agonist force again to compensate for the springlike property of the muscle and minimize the end-point error under SDN. The only noticeable difference in EMG between Fig. 6B and Fig. 2 is that the onsets of the second agonist burst occur earlier in the overshooting case. We also confirmed that the original motor commands of these agonist and antagonist EMG did not overlap.

Keeping other conditions equal, we tested the minimum-energy model, resulting in the kinematics and EMG pattern shown in Fig. 7A and B, respectively. In sharp contrast with results from the minimum-variance model, the velocity profile

was almost symmetric and bell-shaped and no trajectory overshooting was observed. Importantly, the associated EMG pattern of all five muscles showed a homogeneous sustained activity over the movement, which clearly mismatches experimental observations.

Finally, Fig. 8 provides an overview of how the simulated pattern of EMG and trajectory are altered when the viscosity b and stiffness k are varied within the biologically plausible range. The amplitude-graded pattern of EMG was observed uniformly over the full parameter range. On the other hand, the antagonist burst and the trajectory overshooting were more parameter dependent. Antagonist bursts were seen when either the stiffness or viscosity had a comparatively small value. Overshooting occurred only when the stiffness had a large value and viscosity was small.

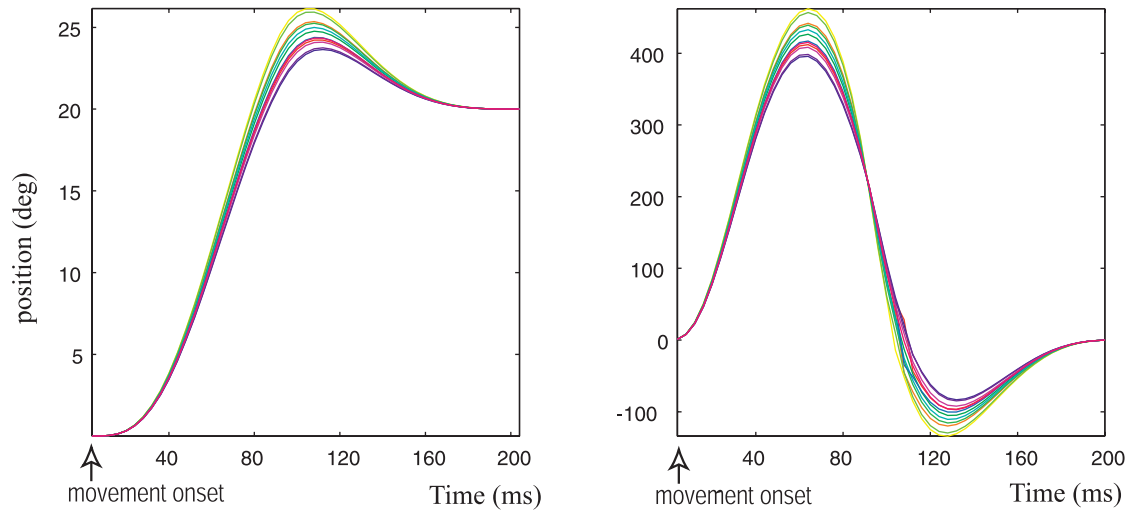
DISCUSSION

In this paper, we have examined an optimal control model of step-tracking wrist movement to probe the computational mechanism that controls the spatiotemporal patterns of redundant muscles' activity. The model that minimizes the end-point variance under SDN successfully captured the most prominent feature of human and monkey EMG data during the step-tracking wrist movement (i.e., amplitude-graded EMG pattern). In addition, the model not only reproduced the cosine-tuning pattern of EMG modulation during both agonist and antagonist burst intervals and the shift of PD from each muscle's pulling direction, but also exhibited overshooting of trajectories, a frequently observed phenomenon in fast wrist movements. These observations are consistent with the view that to recruit redundant muscles accurately, the nervous system optimizes a cost function related to the noise inherent to biological motor system.

Several cost functions can be considered for modeling the step-tracking wrist movements, such as some form of effort minimization. A previous computational model of step-tracking wrist movement minimized squared muscle activation and explained spatial characteristics of cosine tuning of agonist EMG (Fagg et al. 2002). Interestingly, the PDs reported for ECRL, ECRB, ECU, and FCR (e.g., Figs. 4 and 5 in Fagg et al. 2002) were almost the same as those found in the current optimal control study with the minimum-variance and minimum-energy models (Figs. 3 and 4). This similarity of agonist PDs among three different cost functions suggests that the spatial-tuning pattern observed in the step-tracking wrist movement originates from each muscle's pulling direction, rather than a specific cost function and optimization procedure. It was reported in Todorov (2002) that for cosine tuning in the isometric case, minimizing variance under signal-dependent noise is quite similar to minimizing squared controls (the same as our definition of minimum energy model). In comparison with these previous models, the main advantage of the current optimal control approach is the ability to predict a spatiotemporal pattern of EMG and trajectory. The spatiotemporal information is the key not only to study the amplitude-graded pattern of EMG, but also to investigate both agonist and antagonist PDs and the trajectory overshooting.

The cost function we adopted in this study is the end-point variance, where SDN was assumed in each redundant muscle. In comparison with other smoothness-based optimization cri-

A Kinematics



B EMG

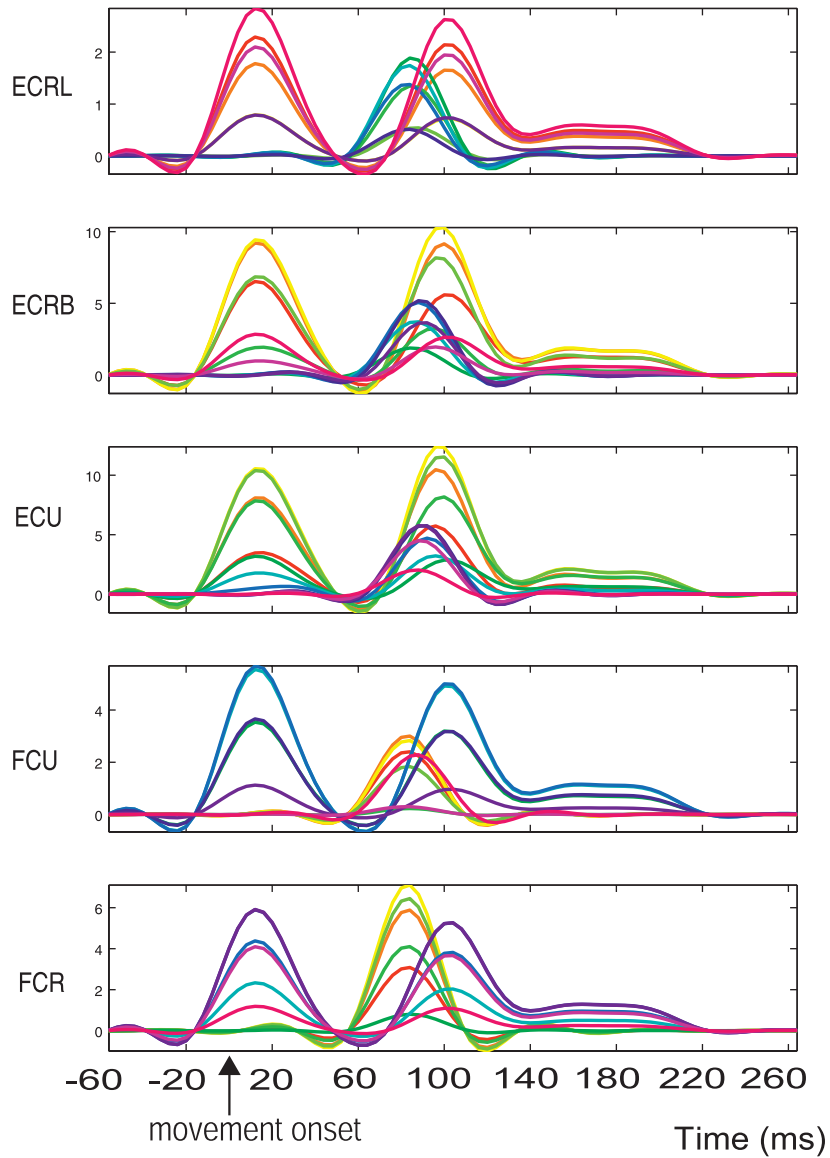
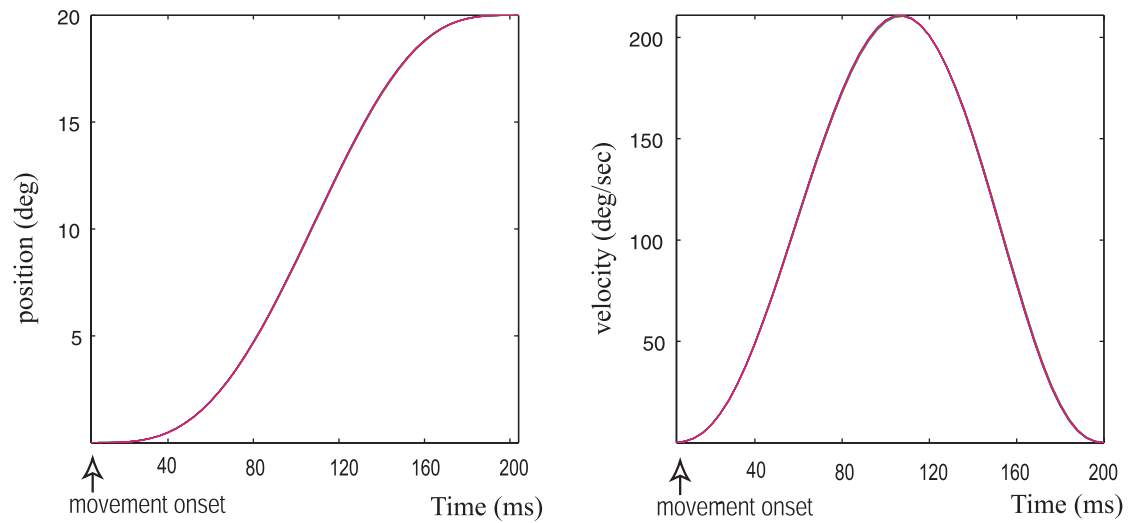


FIG. 6. Prediction by the minimum-variance model under signal-dependent noise (SDN). *A*: trajectories and velocity profiles obtained from the simulation, demonstrating overshooting. *B*: predicted temporal waveform of EMG for ECRL, ECRB, ECU, FCU, and FCR.

A Kinematics



B EMG

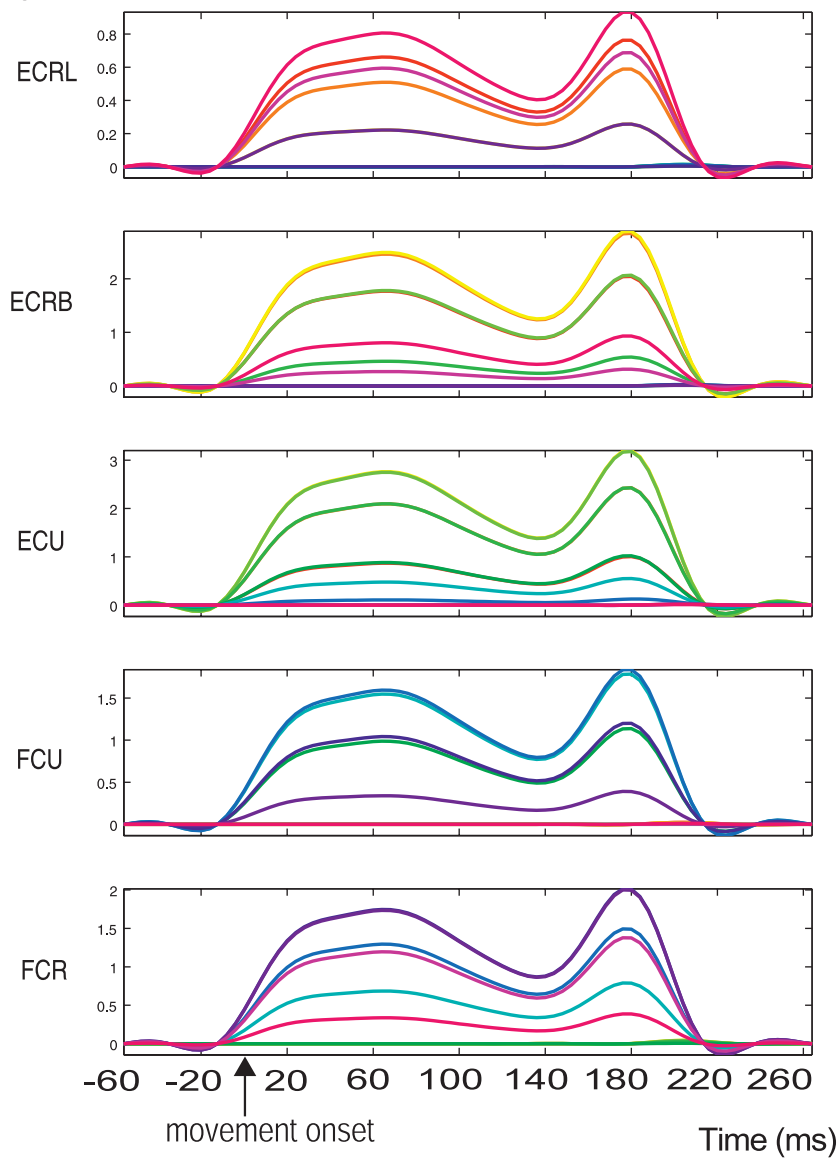


FIG. 7. Prediction by the minimum-energy model. *A*: trajectories and velocity profiles obtained from the simulation. *B*: predicted temporal waveform of EMG for ECRL, ECRB, ECU, FCU, and FCR.

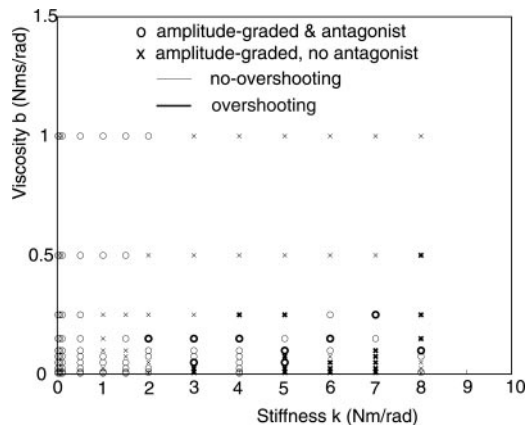


FIG. 8. Effects of stiffness and viscosity on simulated pattern of EMG and trajectory. Stiffness k and viscosity b were varied within the biologically plausible range (inertia was 0.005). Each point in the plot consists of a pair of b and k . Points associated with \circ generated an amplitude-graded burst in agonist and antagonist muscles. Points associated with \times yielded an amplitude-graded agonist burst without an antagonist burst. Thick line indicates b and k values that gave overshoot; thin line indicates b and k values without overshoot. An antagonist burst and trajectory overshooting were considered only when they were clearly visible.

teria to find joint torques for path planning (Flash and Hogan 1985; Uno et al. 1989), SDN proposes that there is noise in muscle force generation whose SD increases linearly with the mean. The origin of SDN was shown to arise within the muscle from the orderly recruitment and firing rate variability of motor neuron pool that innervates each muscle (Jones et al. 2002). Thus when each of redundant muscle is considered in computational modeling, rather than focusing on the aggregates values such as joint torque, SDN-based optimization allows a prediction of muscle activation patterns. It is also demonstrated that a given torque or force can be more accurately produced by a stronger muscle than a weaker muscle, suggesting different strengths and different numbers of motor units cause different amplitudes of motor noise (Hamilton et al. 2004). In the current study, we assumed an identical magnitude of the coefficient of variation (k) for five muscles (ECRL, ECRB, ECU, FCU, and FCR), but it is an interesting future direction to investigate how the number of motor units influences the EMG pattern of redundant muscles whose sizes are fairly different as in whole arm reaching movements, i.e., k is different among muscles. It is also important to note that the predictions of the model is independent of the size of k (provided that k is >0) and the size of k simply scales the overall variability of the movement as the system we model is a linear system.

An interesting consequence arising naturally from the SDN-based cost function is that the target overshooting can be an optimal feedforward control strategy in fast wrist movements. Although at first sight this may appear an unlikely optimal solution, it reflects the model using the passive properties of the wrist to minimize error. In our model, the muscles of the wrist can have a strong passive elastic component. The model uses this feature to reduce variance. By passing the target, the passive elastic properties are used to bring the wrist onto target in the latter half of the movement. Therefore, the motor command, and its associate noise, can be reduced during the latter portion of the movement. Critically, if as a result of the noise the wrist has passed the target by a long way, the wrist

muscles will be substantially stretched and the elastic force will bring the wrist back quickly. However, if because of the noise the wrist has only just passed the target, the muscle is less stretched and the elastic force will bring the wrist back more slowly. Therefore, the spread in possible wrist positions reduces over the latter part of movement arising from these passive properties, make overshooting an optimal strategy.

The minimum-energy model did not produce overshooting nor a biologically realistic EMG pattern in the simulation of overshooting. Generally, models based on a sort of minimizing the energy used, such as minimizing the integrated squared motor command, can never predict overshoot. This can be understood as follows. Assume a minimum-energy model overshoots the target. This means it has zero velocity at a position further than the target. Therefore by scaling down the entire sequence of motor commands appropriately we can arrive stationary at the target location earlier. Moreover, by delaying (moving horizontally) the start of the motor command we can arrive on target at the correct time but clearly now using less energy than the overshooting trajectory. This contradicts the original overshooting trajectory as being minimum energy. The same argument also rules out any cost that penalizes a monotonically increasing function of the motor command equally over the entire movement from producing overshooting. Therefore, a time-varying penalty on the motor command is necessary for overshooting and return to be optimal. This contrast between the SDN-based cost function, which penalizes motor commands differentially over the movement, from minimum energy consumption constraints may indicate an important role of the noise in the biological motor system.

It is certainly a remarkable finding that even with the simple second-order linear muscle and dynamics model used, that we can explain almost all key features of the spatiotemporal patterns of EMG and trajectory overshooting. However, there are some limitations that may require a more realistic nonlinear muscle model (Cheng et al. 2000) and dynamics model. First, the appearance of trajectory overshooting was associated with a comparatively high stiffness. We hypothesize that overshooting can happen even with a lower stiffness in the real nonlinear and activation-dependent dynamics that cannot be captured by linearization (Cheng et al. 2000). A realistic muscle model can also provide a more efficient measure to keep the wrist at the target rather than generating substantial muscle activation after movement. Second, although the amplitude-graded pattern was dominant in EMG modulation (majority of human data and all monkey data), for some muscles and for some selected targets in human subjects, the temporally shifted pattern of EMG was also observed, which is characterized by a gradual change in the timing of a single burst of muscle activity (Hoffman and Strick 1999). This pattern of EMG may contribute to produce a smooth and accurate movement trajectory when subjects need to control redundant nonlinear muscles efficiently. Third, it is difficult for the current model to precisely simulate EMG pattern before the movement onset. This may arise because the simple muscle model does not capture the time delays inherent in realistic excitation–contraction coupling mechanisms.

Finally, although we used a standard quadratic programming technique to optimize our SDN-based cost function, how can it be performed in a biological system? Among many possible implementations, the contrast between feedforward and feedback controllers is critically important (Wolpert et al. 1998). In

general, such an optimization problem as our model can be conducted by either a feedforward controller or an optimal feedback controller that is combined with a predictive forward model (Todorov and Jordan 2002). Todorov and Jordan (2002) proposed that among many possible redundancies, their optimal feedback controller reduces the variance of the dimension that was critical for task performance, whereas the variance of other redundant dimension could increase to compensate for this. Simple wrist movements can provide an ideal place for the interaction between experimental and computational studies on redundancy. For example, it might be possible to examine whether feedforward or feedback controllers are dominant by conducting step-tracking movement experiments, where the target suddenly changes after the presentation of the go signal in some trials. In this setting, the importance of each muscle would vary depending on target and therefore some redundancy criteria should change correspondingly, which can be defined through EMG activity.

APPENDIX: MATLAB CODE OF THE OPTIMAL CONTROL MODEL

```
M=0.200; %movement duration
F=0.500; % holding duration
T=M + F; % Total movement duration
A=20*pi/180; % movement amplitude in radians
dt=M/50; % sampling interval
ts=0:dt:M;
N=length(ts);

musc=5; % number of muscles (ECRL ECRB ECU FCU FCR)
ang=(1.6 18.4 159.5 198.3 304.5)*pi/180; % muscle pulling directions

m=0.005; b=0.03; k=0.1; % wrist dynamics
T1=0.030; T2=0.040; % muscle model time constants
order=4; % order of total system
syms s
w=1/((T1*s+1)*(T2*s+1)*(m*s^2+b*s+k));

p(1)=simple(ilaplace(w)); % impulse response
for i=2:order
    p(i)=diff(p(i-1)); % derivatives of impulse response
end

for dir=1:12
    tang=dir*30*pi/180; % target angle
    % constraints required for final position, velocity and etc.
    for i=1:order
        for j= 1:musc
            w=(j-1)*N+1;
            G(2*i-1,w:w+N-1)=subs(sin(ang(j))*p(i),'t',(M-ts))*dt;
            % x-axis
            G(2*i,w:w+N-1)=subs(cos(ang(j))*p(i),'t',(M-ts))*dt; % y-axis
        end
    end

    b(1)=A*sin(tang); %final x
    b(2)=A*cos(tang); %final y
    b(2*order)=0; % all other states 0
    eq=true(2*order,1); %equality constraints
    z=size(G,2);
    G=[G; eye(z)];
    b(size(G,1))=0;
```

```
eq=[eq;false(z,1)];

for j=1:musc % COST
    w=(j-1)*N + 1;
    p2(w:w+N-1)=subs(p(1)^2,'t',(T-ts));
end
H=diag(p2);

% optimization by quadratic programming
u0=1000*rand(length(p2),1); % initial values
[u,y,ier]=minqdef(u0*0,H,G,b',eq,[],u0)

end
```

ACKNOWLEDGMENTS

We thank Drs. P. Strick, D. Hoffman, and S. Kakei for allowing us to use their pulling-direction data of monkey. We thank Drs. S. Kakei and T. Milner for helpful discussions.

GRANTS

M. Haruno was supported by the Daiwa Anglo-Japanese Foundation.

REFERENCES

- Berardelli A, Hallet M, Rothwell JC, Agostino R, Manfredi M, Thompson PD, and Marsden CD.** Single-joint rapid arm movements in normal subjects and in patients with motor disorders. *Brain* 119: 661–674, 1996.
- Bernstein NA.** *The Coordination and Regulation of Movements.* Oxford, UK: Pergamon Press, 1967.
- Buchanan TS and Shreeve DA.** An evaluation of optimization techniques for the prediction of muscle activation patterns during isometric tasks. *J Biomech Eng* 118: 565–574, 1996.
- Cheng EJ, Brown IE, and Loeb GE.** Virtual muscle: a computational approach to understanding the effects of muscle properties on motor control. *J Neurosci Methods* 101: 117–130, 2000.
- De Serres SJ and Milner TE.** Wrist muscle activation patterns and stiffness associated with stable and unstable mechanical loads. *Exp Brain Res* 86: 451–458, 1991.
- Fagg AH, Sham A, and Barto AG.** A computational model of muscle recruitment for wrist movements. *J Neurophysiol* 88: 3348–3358, 2002.
- Flash T and Hogan N.** The coordination of arm movements: an experimentally confirmed mathematical model. *J Neurosci* 7: 1688–1703, 1985.
- Georgopoulos AP, Kalaska JF, Caminiti R, and Massey JT.** On the relations between the direction of two-dimensional arm movements and cell discharge in primate motor cortex. *J Neurosci* 2: 1527–1537, 1982.
- Gielen GL and Houk JC.** Nonlinear viscosity of human wrist. *J Neurophysiol* 52: 553–569, 1984.
- Grey MJ.** *Viscoelastic Properties of the Human Wrist During the Stabilization Phase of a Targeted Movement* (MS thesis). Burnaby, British Columbia, Canada: Simon Fraser University, 1997.
- Hamilton A, Jones KE, and Wolpert DM.** The scaling of motor noise with muscle strength and motor unit number in humans. *Exp Brain Res* 157: 417–430, 2004.
- Harris CD.** On the optimal control of behaviour: a stochastic perspective. *J Neurosci Methods* 83: 73–88, 1998.
- Harris CD and Wolpert DM.** Signal dependent noise determines motor planning. *Nature* 394: 780–784, 1998.
- Hoffman DS and Strick PL.** Step-tracking movement of the wrist in humans. I. Kinematic analysis. *J Neurosci* 6: 3309–3318, 1986.
- Hoffman DS and Strick PL.** Step-tracking movement of the wrist in humans. II. EMG analysis. *J Neurosci* 10: 142–152, 1990.
- Hoffman DS and Strick PL.** Step-tracking movement of the wrist in humans. III. Influence of changes in load on patterns of muscle activity. *J Neurosci* 13: 5212–5227, 1993.
- Hoffman DS and Strick PL.** Step-tracking movement of the wrist. IV. Muscle activity associated with movements in different directions. *J Neurophysiol* 81: 319–333, 1999.
- Hollerbach JA and Atkeson CG.** Deducing planning variables from experimental arm trajectories: pitfalls and possibilities. *Biol Cybern* 56: 279–292, 1987.
- Jones K, Hamilton A, and Wolpert DM.** The sources of signal-dependent noise during isometric force production. *J Neurophysiol* 88: 1533–1544, 2002.

- Kakei S, Hoffman DS, and Strick PL.** Muscle and movement representations in the primary motor cortex. *Science* 285: 2136–2139, 1999.
- Milner TE.** Adaptation to destabilizing dynamics by means of muscle cocontraction. *Exp Brain Res* 143: 406–416, 2002.
- Milner TE and Cloutier C.** Damping of the wrist joint during voluntary movement. *Exp Brain Res* 122: 309–317, 1998.
- Mustard BE and Lee RG.** Relationship between EMG patterns and kinematic properties for flexion movements at the human wrist. *Exp Brain Res* 66: 247–256, 1987.
- Neumaier A.** General definite and bound constrained indefinite quadratic programming. WWW-Document (<http://www.mat.univie.ac.at/~neum/software/minq/>), 1998.
- Shah A, Fagg AH, and Barto AG.** Cortical involvement in the recruitment of wrist muscles. *J Neurophysiol* 91: 2445–2456, 2004.
- Todorov E.** Cosine tuning minimizes motor errors. *Neural Comput* 14: 1233–1260, 2002.
- Todorov E and Jordan M.** Optimal feedback control as a theory of motor coordination. *Nat Neurosci* 5: 1226–1235, 2002.
- Uno Y, Kawato M, and Suzuki R.** Formation and control of optimal trajectory in human multijoint arm movement. *Biol Cybern* 61: 89–101, 1989.
- Van der Helm FCT and Rozendaal LA.** Musculoskeletal system with intrinsic and proprioceptive feedback. In: *Biomechanics and Neural Control of Posture and Movement*, edited by Winters JM and Crago PE. New York: Springer-Verlag, 2000, p. 164–174.
- Wolpert DM, Miall C, and Kawato M.** Internal models in the cerebellum. *Trends Cogn Sci* 2: 338–347, 1998.